

Causes and control of welding cracks in electron-beam-welded superalloy GH4169 joints

Guo-qing CHEN, Bing-gang ZHANG, Tian-min LÜ, Ji-cai FENG

State Key Laboratory of Advanced Welding and Joining, Harbin Institute of Technology, Harbin 150001, China

Received 6 June 2012; accepted 6 March 2013

Abstract: Welding joint of GH4169 alloy with a good formation was obtained. No macroscopic defects occurred in the joint. The weld had mainly a dendritic structure; the base metal was a solid solution of Ni, Cr, and Fe, and the strengthening-phase particles such as Ni_3Nb were dispersively distributed along the grain boundary. The average tensile strength of the joint reached 743.7 MPa, and the Vickers hardness of the weld exceeded HV 300. Because of the segregation of the low-melting compound Ni_3Nb at the grain boundary of the fusion zone, liquid cracks tended to occur as a result of welding stress. The formation of liquid cracks was inhibited by adding an alloying element, Mn, to the welding bath, because Mn diffused to the fusion zone and the high-melting phase Mn_2Nb formed, and thus the overall properties of the joint were improved.

Key words: GH4169 alloy; electron-beam welding; welding crack

1 Introduction

Superalloys are mainly used in the aerospace, petrochemical, metallurgical, and automobile industries, and are especially important in the aerospace industry. Recently, with rapid aerospace development, the demand for basic research on superalloys has become more urgent [1–4]. GH4169 is a superalloy and is important in aeroengine applications. It has high-temperature strength and excellent corrosion resistance, and it is easy to process at 700 °C and exhibits oxidation resistance at high temperatures. So, it is widely used in various applications with such requirements [5–9]. The practical application of new materials involves joining them, and fusion welding is a relatively good joining method. A comparatively slow welding speed needs to be adopted in laser-beam welding of GH4169, and can achieve a well-shaped welding morphology and avoid the generation of microcracks [10,11]. Microcracks occur easily in gas tungsten arc welding, because the welds have mainly cast structures, which exhibit serious inhomogeneity in components and dendritic structures [12,13]. The characteristics of electron-beam welding are as follows: high energy concentration, high ratio of depth to width of the weld, few welding deformation, and small

welding heat-affected zone (HAZ). The weld morphology and the welding quality can be improved by adding active agents when welding [14,15]. Research on the application of electron-beam welding, a high-efficiency welding method, in GH4169 alloy has been of great significance in the increasing use of this material.

In this study, the microstructure and mechanical properties of an electron-beam-welded GH4169 superalloy were investigated, and the reasons for the generation of liquation cracks in the fusion zone were analyzed. A method of alloying that inhibits crack formation was suggested.

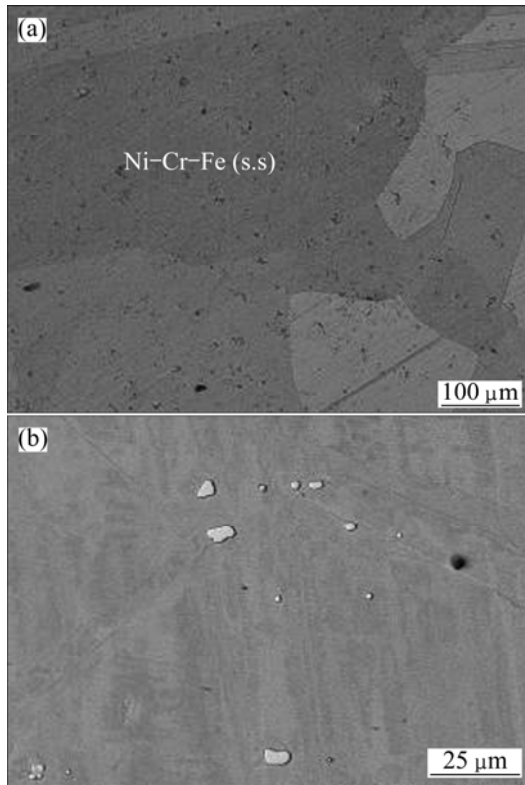
2 Experimental

The base metal used in the experiments was the high-temperature nickel-based GH4169, whose melting temperature and room-temperature tensile strength are 1260–1320 °C and 800 MPa, respectively. The composition of GH4169 is shown in Table 1. The microstructure of the base metal is shown in Fig. 1. The base metal is a solid solution of Ni, Cr and Fe, and a light-colored strengthening-phase, consisting of Ni_3Nb , is distributed in the base metal.

The thickness of the GH4169 alloy plate used in the

Table 1 Elemental composition of GH4169 (mass fraction, %)

C	Cr	Ni	Co	Mo
<0.08	17.0–21.0	50.0–55.0	≤1.0	2.80–3.30
Al	Ti	Nb	Fe	
0.30–0.70	0.75–1.15	4.75–5.50	19.0–20.0	

**Fig. 1** Microstructure of base metal GH4169: (a) Optical microscopy image; (b) Scanning electron microscopy image

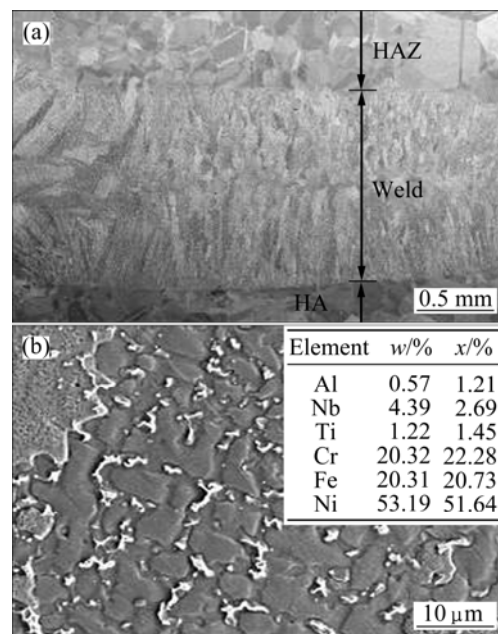
experiments was 6 mm, and it was cut into specimens with dimensions of 60 mm×25 mm×6 mm using wire electrical discharge machining (WEDM) before welding. The sample surfaces were ground and then cleaned with ethanol. The maximum power of the electron-beam-welding gun used in the experiments was 6 kW, and the accelerating voltage, beam current, and welding speed used in the welding process were 55 kV, 25–30 mA, and 8 mm/s, respectively.

After welding, WEDM was used to obtain samples. The joint microstructures were observed using an optical microscope and scanning electron microscope (SEM). The elemental components of the joints were analyzed using energy spectrum analysis and linear scanning, and the phase compositions of the joints were analyzed using X-ray diffraction (XRD). The mechanical properties tests conducted on the joints were room-temperature tensile strength tests, microhardness distribution of the joint cross-section, and observation of the fracture morphology.

3 Results and analysis

3.1 Joint microstructure

The electron-beam-welded GH4169 alloy joints were in good shape, and no macroscopic defects occurred in the joints. The cross-sectional morphology of after welding is shown in Fig. 2(a). It can be clearly observed from the figure that the weld has a cast structure with characteristic columnar grains, whose solidification and crystallization direction is vertical to the fusion line and then grows into the welding bath. During the process of electron-beam welding, the cooling rate of the welding bath is very high and the thermal gradient at the edge of the welding pool is larger than that in the middle. The undercooling degree is inversely proportional to the ratio of the temperature gradient and cooling rate, therefore, coarse columnar grains form near the fusion line but fine dendritic crystals form at the weld center. The HAZ still has an equiaxed grain structure, but the grain is coarser.

**Fig. 2** SEM images showing morphology and microstructure of joint: (a) Cross-section morphology; (b) Weld structure and energy spectrum results

The weld structure is composed of the base metal phase and the light-colored precipitated phase, as shown in Fig. 2(b). The weld has a dendritic structure and the weld grains are significantly refined as a result of the strong agitation of the electron-beam welding bath and the rapid cooling rate after welding. There is some change in the base metal, namely the strengthening-phase is mainly segregated in the interdendritic region and the particle becomes finer. This is because the

cooling rate is so rapid that the strengthening-phase particles have no time to aggregate and grow.

The weld was examined using XRD, and the results are shown in Fig. 3. XRD, combining with the results of energy spectrum analysis indicates that the composition of the substrate phase, which is a solid solution of Ni, Cr, and Fe, is almost the same as that of the GH4169 base metal. The main strengthening-phase in the GH4169 alloy is a body-centered tetragonal γ'' phase (Ni_3Nb), and it also includes the face-centered cubic γ' phase ($\text{Ni}_3(\text{Al,Ti})$) and the δ phase (Ni_3Nb), which is the equilibrium phase of the γ'' phase. These intergranular strengthening-phases are so fine that they have a certain strengthening effect on the welding seam.

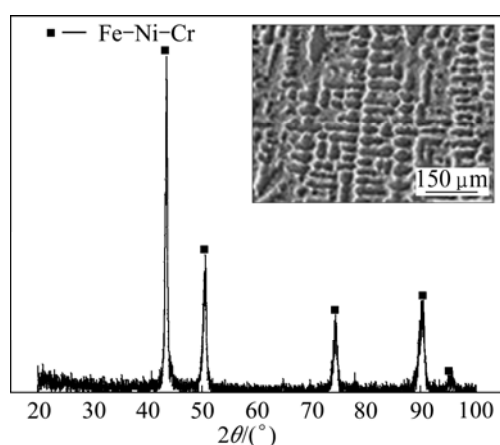


Fig. 3 XRD results of weld

3.2 Causes and prevention of thermal cracks

A well-formed electron-beam-welded GH4169 alloy joint was obtained and the average tensile strength of the joint reached 743.7 MPa, which is close to that of the base metal. However, the Vickers hardness of the welding seam exceeded HV 300, which is significantly higher than the value of HV201 of the base metal, so the coordinate deformation of the joint was weakened. In addition, defects occurred easily in the joint because of the large welding stress induced by the rapid cooling rate of the electron-beam-welded joint.

From microanalysis of the joint after welding, it can be clearly observed (Fig. 4) that microcrack defects occurred at the fusion line near the HAZ. These cracks were intergranular cracks and generally one to two grain boundaries in length; they often occurred at the intersections of grain boundaries. There were many dislocations at the intersections of grain boundaries and they helped to inhibit crack formation. Therefore, some cracks were no longer than the length of one grain boundary. This type of microcrack would not significantly affect the tensile strength of the joint, but would have negative effects on the fatigue properties and corrosion-resistance properties of the joint.

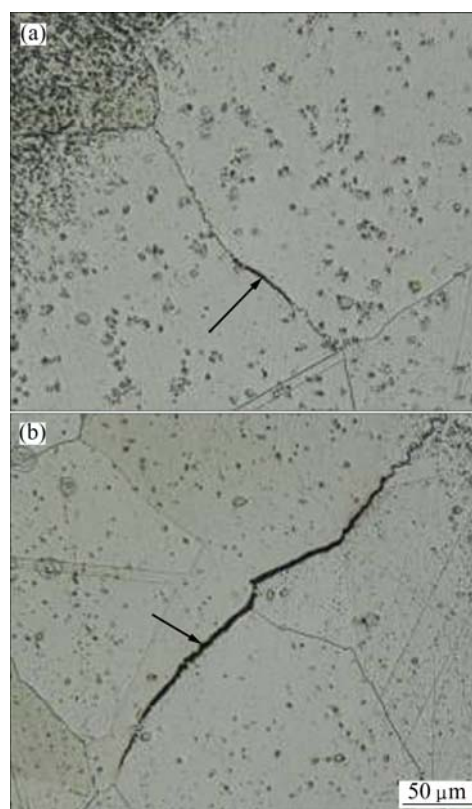


Fig. 4 OM images showing morphology of microcracks at fusion line: (a) Single grain boundary; (b) Boundaries between two grains

There must be connections between the occurrence of intergranular cracks and the weakening of the grain boundary bonding force, therefore the grain boundaries must be carefully analyzed. Analysis using SEM showed that the main reason for the cracks was that there were intermetallics aggregating at some grain boundaries of the fusion zone, as can be clearly observed in Fig. 5. The results of energy spectrum analysis of the intermetallics (Fig. 5(a)) showed that the phase was the γ'' phase (Ni_3Nb) or the low melting (1175 °C) eutectic of δ phase (Ni_3Nb) and Ni_6Nb_7 phase because the intermetallics had high contents of Nb and Ti elements. The γ'' phase aged at 720 °C had a strengthening effect on the alloy. Therefore, the low-melting Ni-Nb compound re-melted under the effects of the welding thermal cycle, and then aggregated at the grain boundaries of the fusion zone, as shown in Fig. 5(b). Besides, large tensile stress formed at the fusion line under the effect of fast thermal cycles. Therefore, as the low-melting eutectic was remelted at the grain boundary, liquation cracks occurred at the fusion line under the tensile stress.

To avoid the occurrence of liquation cracks, the root cause of the cracks should first be investigated. The existence of the low-melting γ'' phase at the grain boundaries caused cracking of the grain boundaries

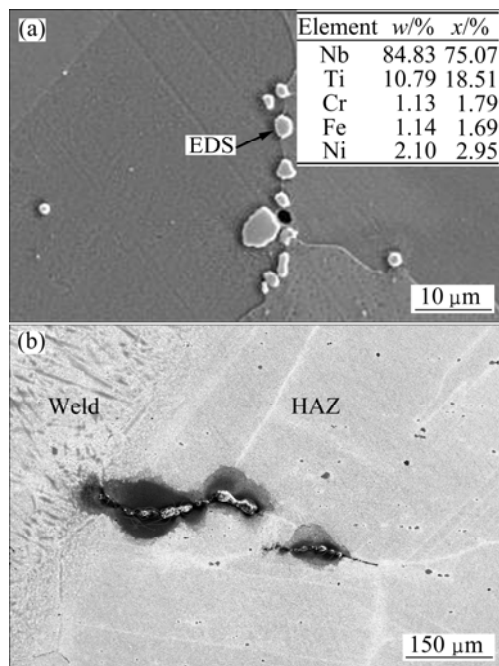


Fig. 5 Aggregation of compounds at grain boundaries of fusion zone by SEM: (a) EDS analysis; (b) Position of compounds

during the cooling process, thus ways of eliminating the Ni_3Nb phase should be considered. Considering that there were certain diffusion reactions at the liquid–solid interface of the fusion line during fusion welding, a new suggestion was put forward. Alloying elements added to the welding bath could diffuse into the fusion zone and high-melting compounds form, substituting the Ni_3Nb phase, and liquation cracks could be avoided.

In selecting the alloying elements, the affinity of the elements with Nb, as well as whether they would have harmful effects, should be taken into consideration, and analysis suggested that Mn should be used as the alloying element. It can be seen from the Mn–Nb phase diagram that when the content of Mn is 27%–33%, the precipitate is Mn_2Nb , whose melting point exceeds 1200 °C and is higher than that of Ni_3Nb . Moreover, Mn can form an infinite solid solution with Cr and Fe, therefore the formation of Ni_3Nb decreased as Mn_2Nb was formed, by increasing the Mn content of the weld seam. However, the Mn content of the weld should be controlled to avoid the formation of Mn–Ni and Mn–Cr brittle phases.

3.3 Research on alloying of weld

In the experiments, a ferromanganese alloy with 75% (mass fraction, %) Mn was added to the joint. By adjusting the welding parameters, a well-formed weld joint was obtained after welding and no macroscopic defects occurred in the joint. The cross-section morphology of the joint demonstrates that the microstructure of the weld was still the equiaxed dendritic structure, and no defects occurred, as shown in

Fig. 6. The XRD analysis results for the joint showed that the weld was still a solid solution of Ni, Cr, and Fe, where the content of Mn was high. According to the results of the energy spectrum analysis, the Mn content of the weld was higher than 40%.

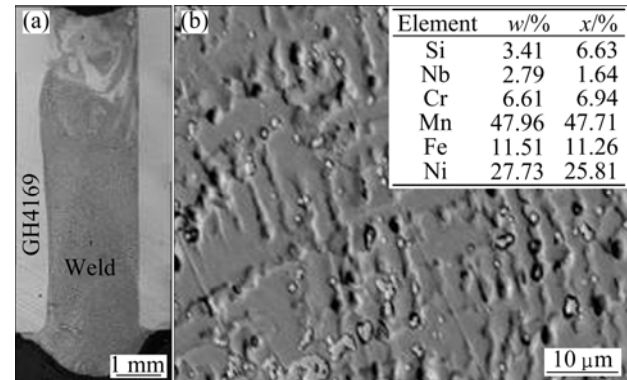


Fig. 6 SEM images showing cross-section of joint (a) and morphology of weld (b)

The Mn content was analyzed from the fusion line to the HAZ, as shown in Fig. 7. It can be seen that the Mn element in the weld fully diffused to the fusion zone, the diffusion distance was more than 200 μm , and the Mn content was about 10%. Diffusion resulted in substitution of Ni by Mn, thus creating the conditions for the formation of the higher-melting Mn_2Nb compound.

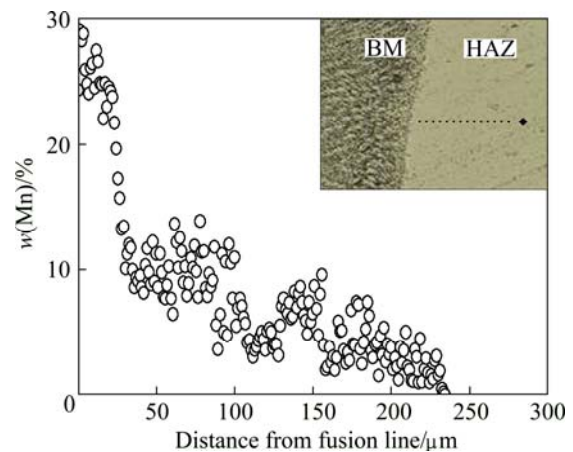


Fig. 7 Distribution of Mn in fusion zone

The welding residual stress could be decreased by increasing the beam current to 30 mA and decreasing the welding speed to 6 mm/s to increase the heat input and decrease the cooling rate during the welding experiments. Moreover, by using scanning function, the Mn element could fully diffuse and well distribute under the intensive stirring effect of the welding pool. The experimental results of the mechanical properties of the weld verified this assumption. It can be clearly observed from the energy spectrum results for the fusion zone that the Mn

content in the crystal boundary compounds was higher than 40%, and the compound can be inferred to be Mn_2Nb , as shown in Fig. 8(a). Thermal cracks did not occur in the joint after weld alloying using Mn, and defect-free joining was obtained. The tensile strength of the joint reached 612.6 MPa after welding, which was 80% of the tensile strength of base metal. The microhardness of the weld was about HV250, which was significantly lower than that of the joint formed by direct welding, and the overall properties of the joint were improved. The fracture mode of the joint after Mn alloying was ductile fracturing, and the fracture surface was dimple fractured, as shown in Fig. 8(b).

In practical applications, under the effect of the joint structure and size, the liquation cracks may be large in size and far from the fusion zone or even extend to the heat affected zone when there is a large welding heat input. In this case, the effect of weld alloying is limited and other measures should be considered. For example, the welding stress at the heat affected zone could be lowered as the cooling rate could be decreased by adding the process of heat treatment after welding. However, all of these methods should be further studied.

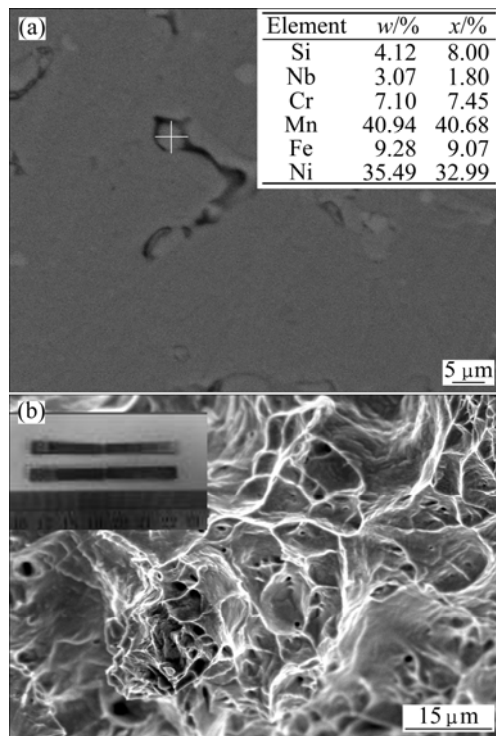


Fig. 8 Energy spectrum analysis and SEM images showing fracture surface of weld

4 Conclusions

1) The electron-beam-welded GH4169 alloy joints were in good shape, and no macroscopic defects occurred. The substrate of the weld microstructure was a solid solution of Ni, Cr, and Fe, and the main

strengthening-phase was Ni_3Nb , which was distributed at the intergrains of the dendrites and had a certain strengthening effect on the weld.

2) Segregation of the low-melting compound Ni_3Nb at the grain boundaries of the fusion zone, together with the stress induced by the welding thermal cycle, caused liquation cracks to form easily in the fusion line.

3) The segregation of Ni_3Nb compound can be avoided by adding Mn as an alloying element to the weld because Mn could diffuse into the fusion zone and form Mn_2Nb . The formation of liquation cracks could therefore be inhibited and the overall properties of the joint could be improved.

References

- [1] REED R C, TAO T, WARNKEN N. Alloys by design: Application to nickel-based single crystal superalloys [J]. *Acta Materialia*, 2009, 57(19): 5898–5913.
- [2] QU F S, LIU X G, XING F, ZHANG K F. High temperature tensile properties of laser butt-welded plate of Inconel 718 superalloy with ultra-fine grains [J]. *Transactions of Nonferrous Metals Society of China*, 2012, 22(10): 2379–2388.
- [3] PINEAU A, ANTOLOVICH S D. High temperature fatigue of nickel-base superalloys — A review with special emphasis on deformation modes and oxidation [J]. *Engineering Failure Analysis*, 2009, 16(8): 2668–2697.
- [4] WANG Z J, GAO T J. Inner and outer pressure forming of nickel based super-alloy thin-walled part with variable diameter sections [J]. *Transactions of Nonferrous Metals Society of China*, 2008, 18(2): 285–290.
- [5] SHANG D G, SUN G Q, CHEN J H, CAI N, YAN C L. Multiaxial fatigue behavior of Ni-based superalloy GH4169 at 650 °C [J]. *Materials Science and Engineering A*, 2006, 432(1–2): 231–238.
- [6] LIU F C, LIN X, ZHAO W W, ZHAO X M, CHEN J, HUANG W D. Effects of solution treatment temperature on micro-structures and properties of laser solid forming GH4169 superalloy [J]. *Rare Metal Materials and Engineering*, 2010, 39(9): 1519–1524.
- [7] LIU Y, WANG L, LIU H Y, ZHANG B J, ZHAO G P. Effect of electropulsing treatment on corrosion behavior of nickel base corrosion-resistant alloy [J]. *Transactions of Nonferrous Metals Society of China*, 2011, 21(9): 1970–1975.
- [8] WANG Z T, ZHANG S H, CHENG M, LI D F, YANG X H. Kinematics and dynamics model of GH4169 alloy for thermal deformation [J]. *Journal of Iron and Steel Research*, 2010, 17(7): 75–78.
- [9] KONG X W, LI B, JIN Z B, GENG W R. Broaching performance of superalloy GH4169 based on FEM [J]. *Journal of Materials Science & Technology*, 2011, 27(12): 1178–1184.
- [10] QU Feng-sheng, ZHANG Kai-feng, LU Hong-jun. LBW/SPF complex forming for multi-sheet structure of GH4169 superalloy [J]. *Journal of Aeronautical Materials*, 2009, 29(4): 5–7. (in Chinese)
- [11] MONTAZERI M, GHAINI F M. The liquation cracking behavior of IN738LC superalloy during low power Nd:YAG pulsed laser welding [J]. *Materials Characterization*, 2012, 67: 65–73.
- [12] WANG Q, SUN D L, NA Y, ZHOU Y, HAN X L, WANG J. Effects of TIG welding parameters on morphology and mechanical properties of welded joint of Ni-base superalloy [J]. *Procedia Engineering*, 2011, 10: 37–41.
- [13] NEMATZADEH F, AKBARPOUR M R, PARVIZI S, KOKABI A H, SADRNEZHAAD S K. Effect of welding parameters on

- microstructure, mechanical properties and hot cracking phenomenon in Udimet 520 superalloy [J]. *Materials and Design*, 2012, 36: 94–99.
- [14] WANG Xi-chang, ZUO Cong-jin, CHAI Guo-ming, ZHANG Lian-feng. Effect of activating fluxes on appearance of weld in thin plate electron beam welding of nickel-base super alloy GH4169 [J]. *Transactions of the China Welding Institution*, 2009, 30(2): 83–86. (in Chinese)
- [15] LIU F Y, YANG C L, LIN S B, WU L, ZHANG Q T. Mechanism of increasing A-TIG welding penetration [J]. *Acta Metallurgica Sinica*, 2003, 39(6): 661–665.

高温合金 GH4169 电子束焊接裂纹缺陷的成因及控制

陈国庆, 张秉刚, 吕天民, 冯吉才

哈尔滨工业大学 先进焊接与连接国家重点实验室, 哈尔滨 150001

摘 要: GH4169 合金电子束焊接接头的成形良好, 无宏观缺陷; 焊缝为树枝晶组织, 基体是 Ni、Cr、Fe 的固溶体, 晶界上弥散分布着 Ni_3Nb 等强化相颗粒; 接头平均抗拉强度达到 743.7 MPa, 但焊缝处的硬度超过维氏硬度 HV 300, 熔合区晶界上低熔点化合物 Ni_3Nb 在此偏聚, 在焊接应力作用下易形成液化裂纹。在熔池中添加合金化元素 Mn, 扩散进入熔合区, 形成高熔点化合物 Mn_2Nb 相, 从而抑制了液化裂纹的产生, 并使接头的综合性能得到改善。

关键词: GH4169 合金; 电子束焊; 焊接裂纹

(Edited by Hua YANG)